A new non-linear limb-darkening law for LTE stellar atmosphere models

Calculations for $-5.0 \leq \log[\mathrm{M/H}] \leq +1$, $2000\,\mathrm{K} \leq \mathrm{T_{eff}} \leq 50000\,\mathrm{K}$ at several surface gravities[*]

A. Claret

Instituto de Astrofísica de Andalucía, CSIC, Apartado 3004, 18080 Granada, Spain

Abstract. A new non-linear limb-darkening law, based on the Least-Squares Method (LSM), is presented. This law is able to describe the intensity distribution much more accurately than any of the old ones given that the differences I(model)-I(fitting) are of some order of magnitude smaller than those derived from other approximations. This new law shows several advantages: it represents well the intensity distribution, the flux is conserved with high accuracy and it permits the use of a single law for the whole HR Diagram since the bi-parametric laws are only marginally valid in certain ranges of effective temperatures. The limb-darkening coefficients are computed for the 12 commonly used photometric bands $uvbyUBVRIJHK$. Bolometric and monochromatic calculations are also available. The computations are presented for 19 metallicities ranging from 10^{-5} up to 10^{+1} solar abundances, with log g varying between 0 and 5.0 and effective temperatures between 2000 K–50000 K. Results for microturbulent velocities of 0, 1, 2, 4, 8 km/s are also available. With this set of data it was possible to investigate, for the first time, the influence of such parameters in the limb-darkening. Limb-brightening, instead of limb-darkening, was detected for some models.

It is shown that the limb-darkening coefficients derived using the Flux Conservation Method (FCM) do not describe very well the intensity distribution, mainly near the border of the disk. On the contrary, the present coefficients, based on the LSM, represent very well the function I(μ) at any part of the disk for any filter or wavelength, log g, effective temperature, metallicity and microturbulent velocity.

The results are presented in 46 tables for the 12 filters (bolometric) and can be retrieved from the CDS. Due to the size of the remaining tables, mainly the monochromatic, these are available only on request (CD ROMs).

Key words: stars: atmospheres – stars: binaries: eclipsing

1. Introduction

The importance of the limb-darkening coefficients (LDC) in light curves analysis of eclipsing binary systems is well known but there are also other fields of the astrophysics where they are essential. Among these additional applications we can quote the studies on the stellar diameters and on the line profiles in rotating stars. A more recent field of research where the LDC is important was explored, for example, by Alcock et al. (1997) who used them in the investigation of the gravitational microlensing. These coefficients are also needed to detect extra solar planets (see, for example, Mazeh et al. 2000).

The list of papers dedicated to the calculation of such coefficients is large and the covered range of effective temperature embraces hot and moderately cold stellar atmosphere models (see for example, Wade & Ruciński 1985; Claret & Giménez 1990; Van Hamme 1993; Díaz-Cordovés et al. 1995; Claret et al. 1995). In a recent paper, Claret 1998 investigated, for the first time, the behavior of intensity distribution for very cold models specially indicated for brown dwarfs (Allard & Hauschildt 1995; Allard et al. 1997; Hauschildt et al. 1997a; Hauschildt et al. 1997b).

In the first attempts to describe the intensity variation over the disk a linear law was used (Milne 1921) and even today, unfortunately, some authors do prefer such an approximation. However, with the advent of more modern stellar atmosphere models it was shown that this simple law was not adequate (Kinglesmith & Sobieski 1970; Manduca et al. 1977; Claret & Giménez 1990; Díaz-Cordobés & Giménez 1992; Van Hamme 1993). Particularly, for very cold models the σ's corresponding to the linear approximation may be as high as 0.15 (Claret 1998).

Once accepted that the limb-darkening is not a linear phenomenon, alternative laws were proposed: quadratic (Manduca et al. 1977; Wade & Ruciński 1985; Claret & Giménez 1990); square root (Díaz-Cordovés & Giménez 1992); logarithmic (Kinglesmith & Sobieski 1970). These laws are represented by the following equations:

Linear

$$\frac{I(\mu)}{I(1)} = 1 - u(1 - \mu) \tag{1}$$

Quadratic

$$\frac{I(\mu)}{I(1)} = 1 - a(1 - \mu) - b(1 - \mu)^2 \tag{2}$$

Square root

$$\frac{I(\mu)}{I(1)} = 1 - c(1 - \mu) - d(1 - \sqrt{\mu}) \tag{3}$$

Logarithmic

$$\frac{I(\mu)}{I(1)} = 1 - e(1 - \mu) - f\mu\ln(\mu) \tag{4}$$

where I(1) is the specific intensity at the center of the disk, u, a, b, c, d, e, f are the corresponding LDC and $\mu = \cos(\gamma)$, γ being the angle between the line of sight and the emergent intensity.

On the other hand, the numerical method used to compute the LDC was always matter of discussion. Grygar (1965), Grygar et al. (1972), Manduca et al. (1977), Claret & Giménez (1990), Díaz-Cordovés et al. (1995), Claret et al. (1995), Claret (1998) adopted the Least-Square Method. Another method, based on the flux conservation, was used for example by Kinglesmith & Sobieski (1970), Wade & Rucisńki (1985) and Van Hamme (1993).

In this paper we present a new non-linear approximation for the specific intensity distribution which describes it very accurately and as a consequence, the flux is conserved with high accuracy. In fact, even for a few worse fitting, the flux is conserved with a mean accuracy better than 0.05 per cent. The least-squares method (LSM) was used to fit the model specific intensity distribution. In Sect. 2 we describe the details of the computational method to derive the LDC and Sect. 3 is devoted to analyze the results and compare them with previous calculations, mainly those based on the flux conservation method (FCM). Finally, we give in Sect. 4 a summary of the available data and how they can be retrieved.

2. Numerical method and the models of stellar atmosphere

Before applying the LSM, we integrate the specific intensities for each μ for the most commonly used photometric passbands $uvbyUBVRIJHK$ following the equation:

$$I_a(\mu) = \frac{\int_{\lambda_1}^{\lambda_2} I(\lambda, \mu)S(\lambda)d\lambda}{\int_{\lambda_1}^{\lambda_2} S(\lambda)d\lambda} \tag{5}$$

where $I_a(\mu)$ is the specific intensity in the band a, $I(\lambda,\mu)$ is the monochromatic specific intensity and $S(\lambda)$ is the response

function which considers the terrestrial atmospheric transmission, filter transmission curves, detector sensitivity and reflection from the aluminum coated mirror. Atmospheric transmission and reflection from aluminum mirror were taken from Allen (1976). For R and I, the transmission curves were taken from Bessel (1990) and the sensitivity of the CCD Tektronics was taken from Peletier (1994). For J, H, and K, the transmission curves were taken from Alonso et al. (1994) (the sensitivity of the In-Sb detector has been included). A small dependence with the spectral type of the effective wavelength was detected for the filters $RIJHK$. The sensitivity of the detectors must be compatible with the transmission curves of the filters since, in general, older detectors are not sensitive in the ultraviolet and/or in the infrared. The monochromatic calculations were performed following their classical definition.

2.1. A new non-linear law

It is known that the behavior of the distribution of the specific intensities depends on the effective temperature and local gravity. For example, Díaz-Cordovés (1990) concludes that the square root law is more adequate to hot stars while for colder ones the quadratic approximation represents the distribution better. Only for effective temperatures of the order of 5500 K the linear approximation can be considered as marginally good. Similar conclusions were obtained by different authors too. It is then clear that it would be very useful a single and accurate law for the whole spectrum of effective temperature and gravities. In order to improve the situation we introduce in this paper a new non-linear law which, as we shall see later, is capable of reproducing the specific intensities over the whole disk and that simultaneously preserves the flux with high accuracy.

The law that we propose can be written as

$$\frac{I(\mu)}{I(1)} = 1 - a_1(1 - \mu^{1/2}) - a_2(1 - \mu) - a_3(1 - \mu^{3/2}) - a_4(1 - \mu^2) \tag{6}$$

or, in a more compact form

$$\frac{I(\mu)}{I(1)} = 1 - \sum_{k=1}^{4} a_k(1 - \mu^{\frac{k}{2}}) \tag{7}$$

A criticism one can make on such an approximation is that now we have four coefficients instead of one or two. However, this is the price one has to pay to describe correctly a non-linear phenomenon. As shown in previous works, simple laws with two coefficients are not good enough to reproduce the intensities though they do it better than the linear one. Even in the hypothetical case that such laws could do it, there is not a single law, i.e., one has to separate the HR diagram in "laws" in order to use the LDC adequately. Moreover, Eq. (6) produces σ's of the order of 2 magnitudes smaller than any of the laws quoted previously. The implementation of this equation in the codes of light curve synthesis is easy as well as in the other fields of the astrophysics where the LDC are need. The apparent complexity of Eq. (6) is highly compensated by accurate calculations and

by the use of a single law for the whole HR diagram. In fact, the four coefficients are not an extra weight to light curves investigators. The modern light curves codes tend to process all the information from the atmosphere models and, in the near future, the LDC may be even computed internally by those codes.

At first sight, it would seem that just by increasing the number of parameters or the degree of the polynomial, we would get better matches to the intensity distribution. We have performed some numerical experiments to investigate that. For example, if we take the expression $1 - \sum_{k=1}^{4} a_k (1 - \mu)^k$ the resulting σ's are higher than those with Eq. (6). Others combinations yield similar results.

2.2. Least-squares and flux conservation methods

The controversy on the best method to derive the LDC is an old matter of discussion. Summarizing the question, the LSM gives a better fit to the intensity distribution but the resulting flux, as computed using the fit, does not always equal the actual flux obtained directly from the model. On the other hand, the flux conservation method (FCM) uses this constraint to derive the LDC. However, although by definition the flux is conserved, the distribution of the intensities is not well described as required and the respective σ's are usually high, mainly near the limb.

The disagreements I(model) - I(fitted) derived from the LSM and FCM formulations are often only qualitatively discussed. In the present work we shall present an exhaustive analysis of this crucial point. As we will see later, the σ's associated to the FCM are as large as 1000 times those provided by the LSM and Eq. (6). This is a serious restriction to the FCM since a good match is necessary to compute the loss (gain) of light during the eclipses, for example. Another weak point of the FCM is that if a non-linear law is used, an extra condition must be introduced. Often, this extra condition is arbitrary: some authors imposed that the limb-darkening law in question should produce the same mean intensity as the atmosphere model. Others make use of a different procedure. This implies that the derived LCD will depend on the selected extra conditions.

The FCM does not make use of any direct information on how the specific intensity is distributed over the disk; its contribution is realized only through integrations. An additional criticism to the FCM is that it does not distinguish, a priori, one law from another since for any adopted law (linear or not) the flux is conserved. The users of such a numerical procedure have to use the corresponding σ's to select the best law. It is interesting to note that the σ test is then decisive whereas it is not when comparing the capability of reproducing the specific intensity distribution of the two competing numerical methods.

It is important to keep in mind that not only the flux conservation is essential to any limb-darkening law. That law must match two conditions: it must be capable of describing accurately the intensity distribution when the stellar disk is scanned and this must lead to the flux conservation. The FCM, by definition, is only capable of fulfilling the second condition. Once obtained, the LCD cannot be adjusted to improve the fitting to the model intensities. On the other hand, the LSM, using an adequate law, can fulfill both conditions. Therefore, we search for a compromise between the best fit to the points and the flux conservation within a small tolerance limit. One should criticize this numerical limitation but it should be remembered that this concept, flux conservation, must be considered with care. In order to check the accuracy of the actual flux calculation, we have performed some numerical experiments by changing the number and position of the μ points. The results, based on the ATLAS grid with log [M/H] = 0, reveal that the errors introduced in the actual fluxes due to these changes are of the same order – sometimes much larger – as the differences between the actual fluxes and those computed using the new limb-darkening law. Other numerical limitations are recognized even by the FCM users (see Wade & Ruciński 1985) who found differences sometimes larger than 2 per cent between the fluxes they computed and those provided directly from the Kurucz's grids (1979). Such numerical limitations shall restrict the flux conservation within certain tolerance, which obviously must be as small as possible. Remember that the numerical limitations due to the flux calculations also affect the LDC computed following the FCM.

With these remarks on mind, we decide to adopt the LSM in the present work using the new law expressed by Eq. (6). One is interested in a approximation that:

1. uses a single law which would be valid for the whole HR diagram
2. would be capable to reproduce very well the intensity distribution
3. the flux would be conserved within a very small tolerance
4. would be applicable to different filters as well as to monochromatic values
5. would be applicable to different chemical compositions, effective temperatures, local gravities and microturbulent velocities.

2.3. Description of the stellar atmosphere models

We shall use an extensive amount of data which we separate following their origin. In all cases the adopted geometry is plane-parallel. Hydrostatic equilibrium and LTE are assumed. Most of these comprehensive data were derived from the ATLAS code and were kindly prepared for the present work by Kurucz (2000). It should be emphasized that such ATLAS models incorporate several improvements with respect to the 1993 set. The effective temperatures are between 3500 and 50000 K with log g varying from 0.0 up to 5.0. The adopted mixing-length parameter was 1.25 and 1221 wavelengths were used at 17 values of μ. The present calculations are not limited to the solar composition but they were also performed for 19 metallicities. The logarithms of the metal/hydrogen ratio are: –5.0, –4.5, –4.0, –3.5, –3.0, –2.5, –2.0, –1.5, –1.0, –0.5, –0.3, –0.2, –0.1, 0.0, +0.1, +0.2, +0.3, +0.5, +1.0, for a microturbulent velocity of 2 km/s. With these characteristics it will be possible, for the first time, to study systematically the influence of the metal content on the LDC. Of course, the importance of this fact is not only in the theoretical intercomparison but also under the observational point of view

view given that observations of eclipsing binaries and gravitational micro-lensing investigations are now being carried out in chemical environments different from the solar one. For the solar abundance, calculations were performed for four additional values of the microturbulent velocity: 0, 1, 4 and 8 km/s. With this comprehensive set of data it is possible to analyze the influence of this parameter on the LCD. There are about 400 models for each metallicity, completing about 9500 models.

The second set of models is derived from the PHOENIX code and they were the subject of a previous study (Claret 1998) but they were included here in order to test the law proposed in Eq. (6) at temperatures lower than in the ATLAS grid. Moreover, we will also compute the monochromatic and bolometric LCD for such models since in the mentioned work only the results for 12 passbands were presented. Let us remember some of its basic input physics. One hundred molecules and about 2 million atomic lines were included. Dust formation and dust opacities are not taken into account. This affects mainly models with effective temperature smaller than 3000 K. The range of effective temperature is 2000 K $\leq$ log T_{eff} $\leq$ 9800 K and log g is between 3.5 and 5.0 and only models with the solar metallicity were considered. The selected mixing-length parameter was 1.0 and the microturbulent velocity is 2 km/s. The number of wavelengths is 5399 ranging from 300 nm up to 2999.5 nm. The number of emergence angles is similar to that of ATLAS (16).

3. Discussion of the results

In Sect. 3.1 we analyze the results for the ATLAS models concerning the 12 passbands and the monochromatic calculations. In addition, we discuss the monochromatic comparison of the LSM and FCM results for the Sun while the models calculated with the PHOENIX code will be the matter of the Sect. 3.2.

3.1. The effects of metallicity and microturbulent velocity on the LDC: ATLAS models

Let us first check if the new approximation we have proposed fulfills the requirements described above. In order to do that, we shall use two criteria: the σ merit function and the flux conservation. We emphasize that the flux conservation in our formulation is a consequence of the goodness-of-the-fit and it is not imposed a priori. The merit function is written as

$$\sigma^2 = \frac{1}{N-M} \sum_{i=1}^{N} (y_i - Y_i)^2 \qquad (8)$$

where y_i is the model intensity at the point i, Y_i the fitted function at the same point, N is the number of points and M is the number of coefficients to be adjusted.
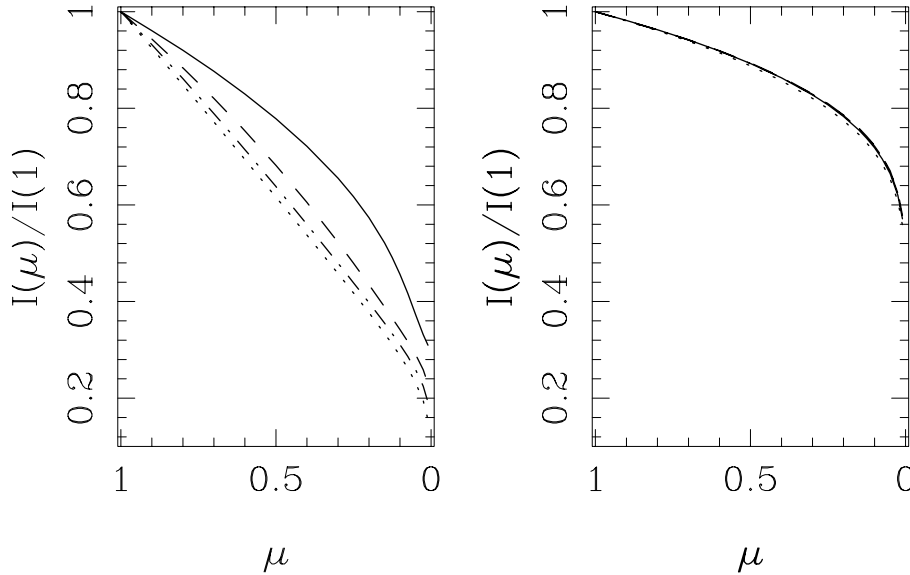
In order to compare the LSM and FCM results, we define the function σ_r which gives the ratio of the σ's obtained using the FCM and LSM. The upper panels in Fig. 1 show the resulting log σ_r for the 12 passbands, including all available values of log g, log T_{eff} and for 9 values of log [M/H] (around 400

models per metallicity). It is clear that the quality of the LSM fitting is much better than that obtained with FCM for any filter, metallicity, effective temperature or log g. In some cases, the ratio can achieve 1000. We have adopted the logarithmic approximation for the FCM case but similar results are derived when considering the root square or quadratic approximation. The accuracy of the fitting can be also translated to the parameter $F_a/F_{a,limb} \equiv F'/F$, the ratio of the actual flux at the passband a and that using the new limb-darkening law. Those ratios, again for the 12 filters, log g, log T_{eff} and 9 values of log [M/H], are drawn in the lower panels in Fig. 1. The flux conservation is guaranteed within a high precision. The worst points correspond generally to convective models with log $T_{eff} \leq 3.9$. The maximum difference is smaller than 0.0005, a result certainly better than those obtained with any bi-parametric approximations and perfectly within the current numerical limitations. It should be also mentioned that a slightly larger scattering is detected for less metallic models.

In Fig. 2 we can inspect directly how the angular intensity distribution depends on the metallicity for a few models. Note that there are changes in the behavior of the model with $T_{eff} = 5000$ K when going from smaller to higher metallicities. The angular distribution is more pronounced for more metallic models, that is, the linear component predominates. For high effective temperatures, the dependence with the metal content is not so large. Fig. 3 displays how a_1, a_2, a_3 and a_4 depend on the metal content and effective temperature for a fixed value of log g. For the half-integral values of the exponent of μ in Eq. (6), the corresponding coefficients increase with the metallicity while for the integer ones the contrary occurs. As pointed out above, the LDC for hot models do not depend strongly on the metallicity. The behavior of the LDC is more complicated when one goes from the hot models to cold ones. The discontinuity, around log $T_{eff} = 3.9$ is detected as already noted by Díaz-Corbovés et al. (1995) (their Fig. 11) and Claret et al. (1995) (see their Fig. 1). However, such a gap is a characteristic of the atmosphere models themselves: it is due to the onset of convection. Note that the discontinuity in the a_i is dependent on the metal content, being relatively smaller for more metallic models. This discontinuity depends also on the passband, being smaller for the larger effective wavelengths. In Fig. 4 we can see in more detail the influence of the metallicity on the LCD for some selected models. For the models with $T_{eff} = 10000$ K and 20000 K, the coefficients are practically independent of the metallicity if, log [M/H] < −2.

The influence of the microturbulent velocity on the LDC can be examined by inspecting Fig. 5. As expected, the contribution of the microturbulent velocity is small for the hotter models. For this reason, we only draw the results for the colder ones. The a_1 and a_3 coefficients increase as the microturbulent velocity increase. A similar effect occurs if the metallic content is increased for a fixed microturbulent velocity.

With reference to the Sun, we have performed monochromatic and band calculations in order to compare with the results obtained with the FCM. The first two frames in Fig. 6 illustrate the angular distribution of the intensities for two wavelengths:

Fig. 2. The angular distribution of the specific intensity as a function of the metallicity for models with T_{eff} = 5000 K (left) and 30000 K (right) for log g =4.5. Continuous line denotes log [M/H] = -3.0, dashed log [M/H] = -1.0, dotted-dashed log [M/H] = 0.0 and dotted log [M/H] = +1.0. ATLAS models, microturbulent velocity = 2 km/s. Filter y.

220.5 nm and 2545 nm. The asterisks represent the fit using Eq. (6) while crosses denote the logarithmic law as computed following the FCM. The superiority of our proposed law can be clearly seen. The corresponding flux ratios, F'/F, are 1.0005 and 0.99994 respectively, perfectly within the flux conservation criterion. The F'/F ratio is very good also for other spectral regions as we can see in the third frame of Fig. 6. The high level of disagreement between the intensities model and those computed following the FCM prescription can be checked in the fourth frame of the Fig. 6. We have plotted the difference between the fitted intensity near the limb (for μ=0.01) and that extracted directly from the atmosphere model for the Sun as a function of the wavelength. The quality of our fitting (dashed line) if compared with the FCM one (continuous line) is obvious. The FCM produces discrepancies as large as 0.3 at the ultraviolet. Such differences are smaller for larger wavelengths but they are always larger than those derived using the LSM and Eq. (6). On the contrary, the LSM gives a very good fit for any spectral region. Similar behavior was found for other ints of the disk.

Note that the logarithmic LDC as computed using FCM (first frame of Fig. 6) predicts a limb-brightening at λ = 220.5 nm for the solar model, which is in contradiction with the actual intensities. However, limb-brightening can be effectively found for some models. For example, for log [M/H] = -5.0 we have identified this effect for several wavelengths between 23 and 509 nm for effective temperatures between 4250 K and 50000 K. The fifth frame of Fig. 6 shows the intensity distribution for a model with T_{eff}= 10500 K, log g = 4.5 and λ = 106.5 nm. Although the effect of limb-brightening is not too large, it can be easily observed in that figure. The limb-brightening we have detected in this model may not be real (Kurucz 2000). Real limb-brightening, may be present in irradiated atmospheres. In 1990 and 1992, Claret & Giménez studied the effects of irradiation on the limb-darkening, effective temperatures, albedo, etc. Under those conditions of irradiation, they have not found
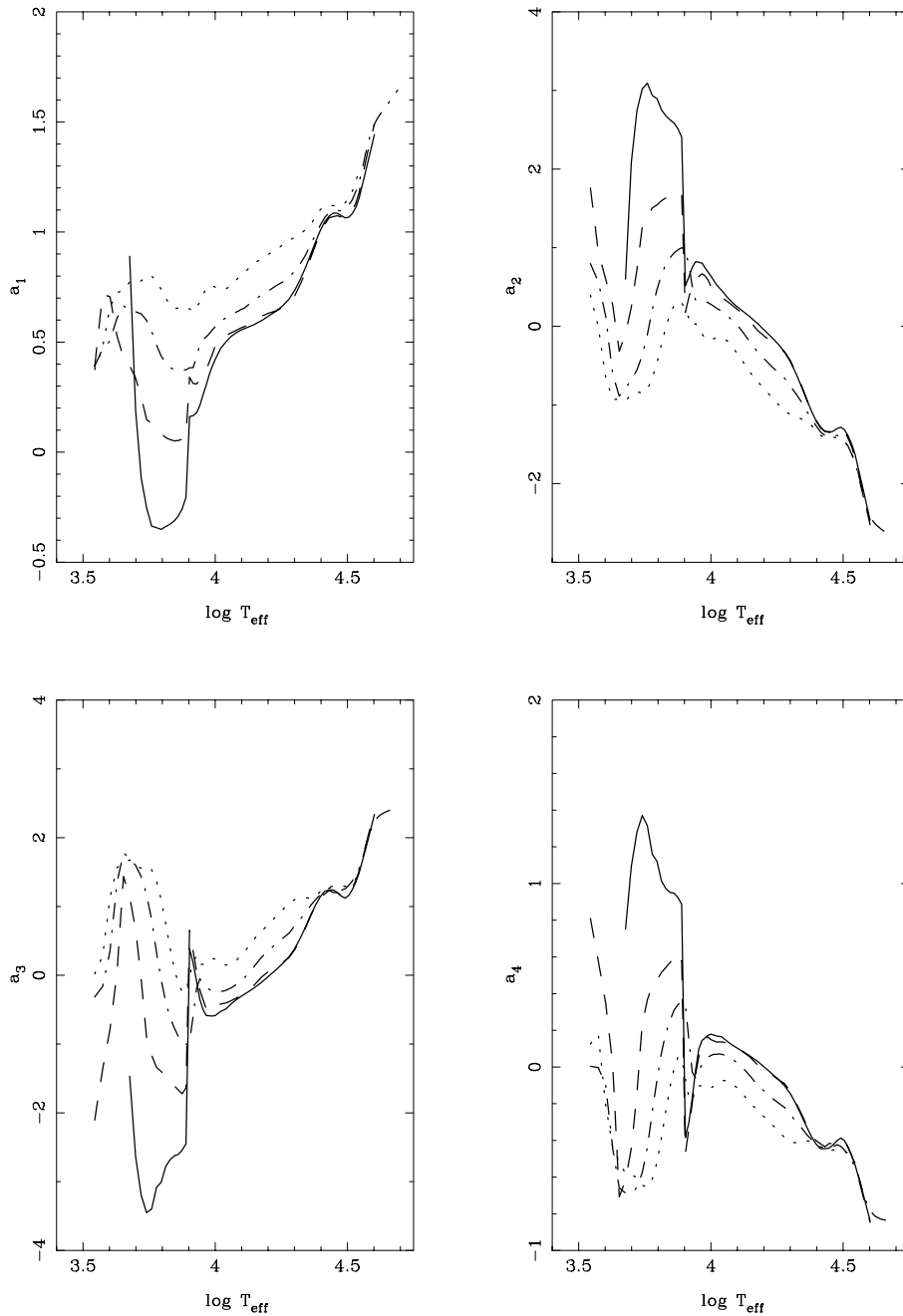
limb-brightening in their irradiated models. They only quoted a tendency of the intensity distribution of an irradiated atmosphere to be more uniform. In fact, none of their figures indicated limb-brightening since the intensities in the outer parts of the disk are always smaller or, at least, equal to the previous points. Buerger (1972) found a similar effect.

3.2. PHOENIX models:
monochromatic and 12 passbands calculations

The same numerical procedure was used to investigate the angular distribution of the intensities for the PHOENIX models. In the upper panels in Fig. 7 we represent log σ_r against log T_{eff}. All available values of log g for the 12 filters are plotted. Again, the superiority of Eq. (6) and of LSM fitting is notorious given that log σ_r, as in the case of the ATLAS models, can achieve 3 orders of magnitude in some cases. The lower panels in Fig. 7 allow us to inspect the quality of the fitting on the ratio of the fluxes. In fact, the worse value of this ratio is around 0.9998. Within this numerical discrepancy, we can consider that the requirement of the flux conservation is fulfilled by Eq. (6) also for the PHOENIX models for the 12 passbands.

The monochromatic calculations required more than 750000 individual fits ranging from 300 nm up to 2999.5 nm. The goodness-of-the fit is somewhat inferior to the band matches but they are perfectly acceptable. In the upper panels in Fig. 8 we show how the flux ratios depend on the wavelength for four selected models with effective temperatures of 4600 K, 5400 K and 8000 K. The fittings are almost perfect for the hotter models for all wavelengths considered. For colder models, there is a dependence of the fitting quality with λ. For shorter wavelengths, F'/F depends on the spectral region in a more complicated way. These remarks indicate that there is not only a dependence of the fluxes ratio with λ but also with the effective temperatures. On the other hand, by comparing the first and the second frames of the Fig. 8 we note a slight dependence of F'/F on log g since

Fig. 3. The four LDC as a function of log T_{eff} and metallicity. The symbols have the following meaning: (continuous) log [M/H] = -5.0; (- - -) log [M/H] = -1.0; (-. -.) log [M/H] = 0.0; (....) log [M/H] = +1.0. Results for the y filter and log g = 4.5. ATLAS models, microturbulent velocity=2 km/s.
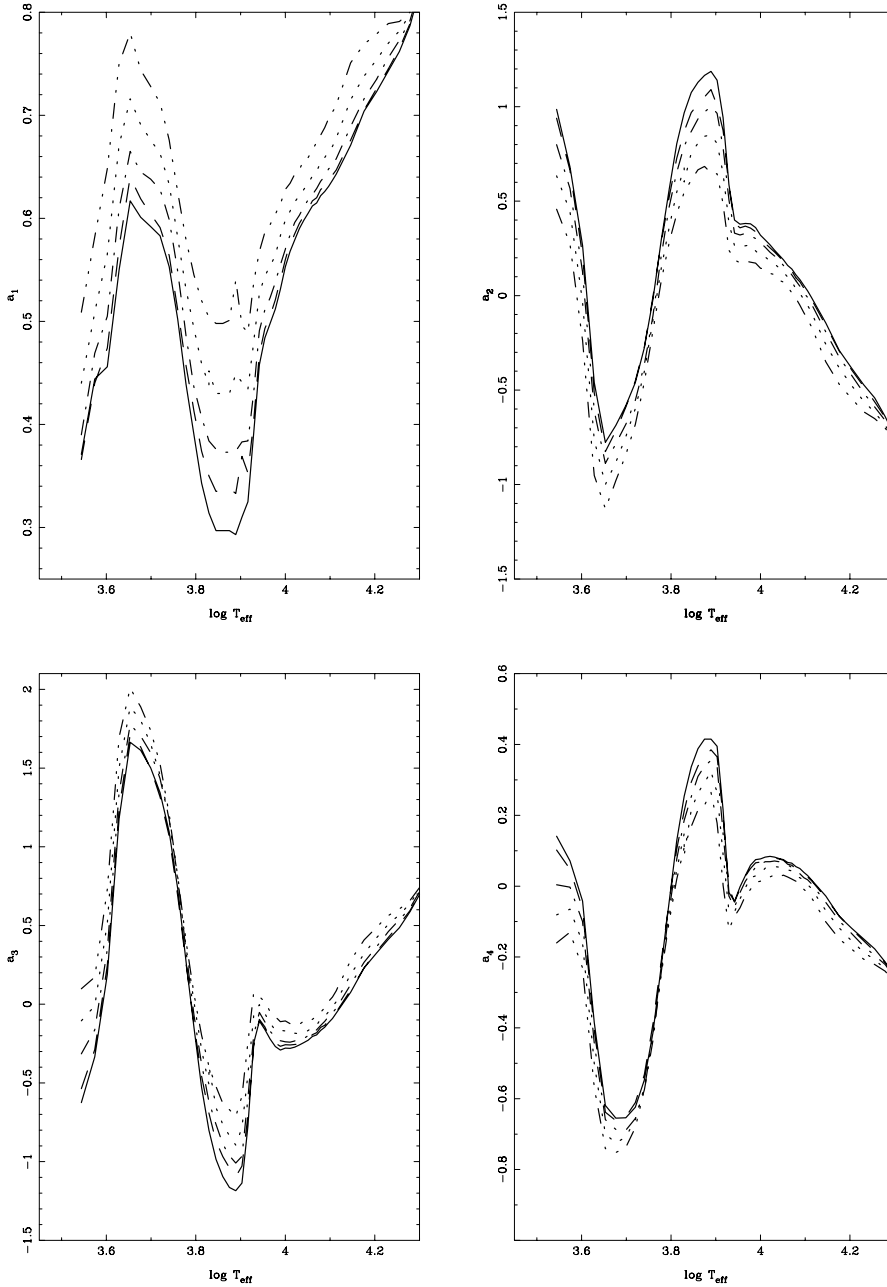
for the visible this ratio approximates a little more to the unity for the model with smaller radius.

The lower panels in Fig. 8 show the fitting quality using LSM and FCM for the same models at $\mu = 0.005$, that is, near the border of the disk. As previously commented, this is a crucial test. It clearly shows, once again, the superiority of the LSM against FCM predictions. Therefore, also for the PHOENIX models, the use of LDC based on the FCM may introduce severe errors. The high quality of the fitting provided by LSM guarantees that the flux is conserved within a desired accuracy and simultaneously that the procedure is able to describe very well the intensity distribution at the limb as well as in any part of the disk for any passband or wavelength.

As a final remark, it should be mentioned that limb-brightening was detected for some colder models ($T_{eff} \leq 2600$ K). However, as commented in Sect. 2.3, the models in this range of effective temperature are not enough realistic. The CH_4 may cause temperature inversions which would be responsible for the limb-brightening (Hauschildt 2000).

4. Tables organization and final remarks

The amount of data resulting from the present calculations is too large. For this reason, we decided to distribute through CDS only part of these tables. The remaining data can be sent to interested readers upon request (they will be available on CD

Fig. 5. The influence of the microturbulent velocity on the coefficients of Eq. (6). The symbols are: (continuous, 0 km/s), (- - -, 1 km/s), (-.-, 2 km/s), (..., 4 km/s) and (-...-, 8 km/s). The represented models have log g = 4.5. Filter y.

ROMs). Table 1 summarizes the characteristics of the results which can be retrieved directly from the CDS.

The data available on separate CD ROMs are the following:

1. same set as described in Table 1 but with monochromatic calculations using Eq. (6).
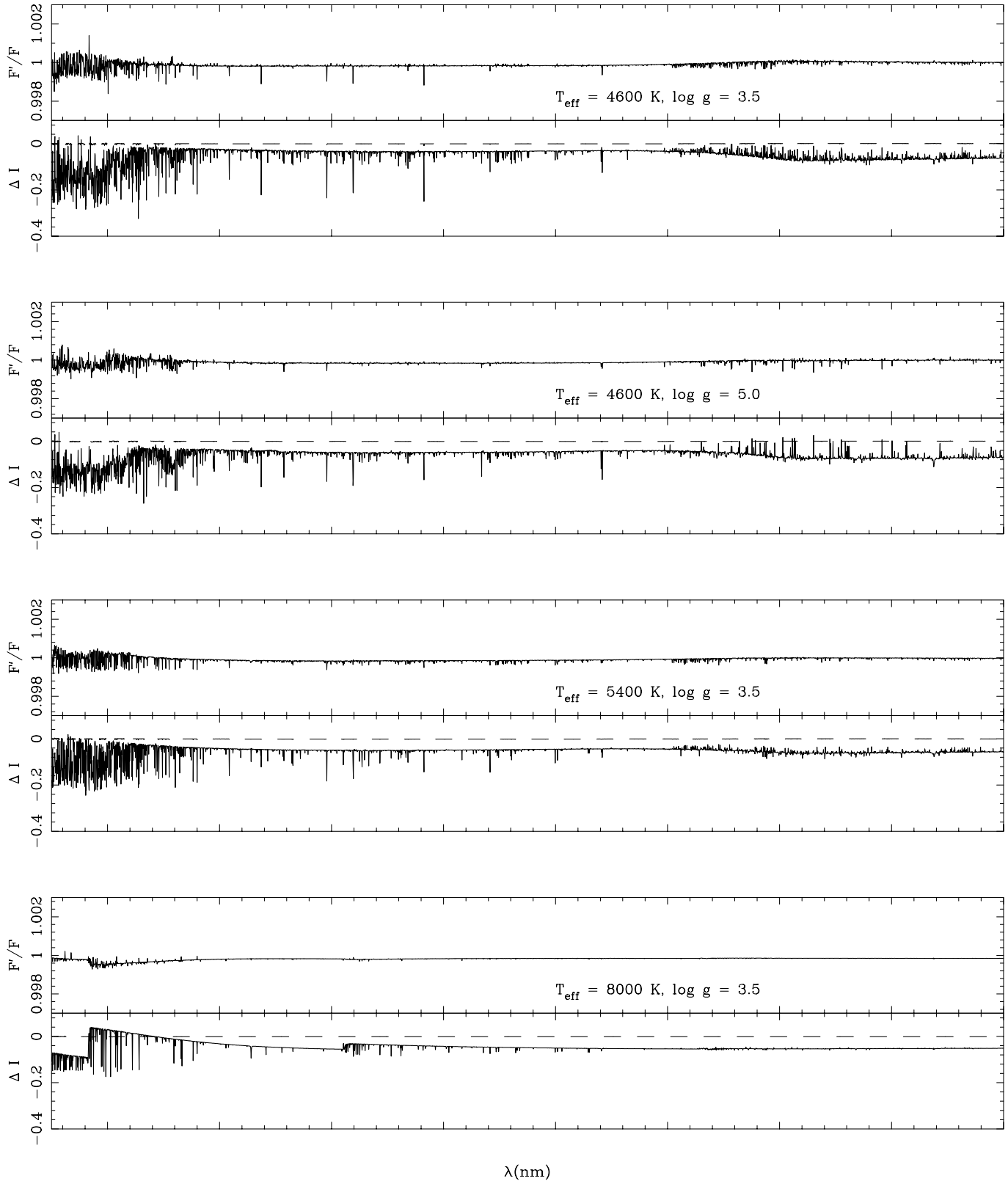2. same set as described in Table 1 but using Eqs. 1, 2, 3, 4.

In spite of the problems in the LDC computed applying the FCM that we have discussed, we will make available to interested readers the same set as described in Table 1 but using Eqs. 1, 2, 3, 4 and FCM for the passbands ($uvbyUBVRIJHK$). Monochromatic and bolometric calculations will be available only on request.

As mentioned in Sect. 2.1, modern light curves codes try to use as much information as possible from the stellar atmosphere models. In order to contribute to this, we will make available complementary tables containing the actual model intensity distribution for the 12 passbands for each grid described in Table 1.

Finally, it should be pointed out that additional features may appear in the LDC for eclipsing binaries if the mutual irradiation of the components is considered (Giménez & Claret 1989; Claret & Giménez 1990, 1992). An irradiated stellar atmosphere will present a different distribution of brightness if compared with standard models without an external radiation field. In the present work, we only present the results for non-irradiated models. The influence of the external radiation field will be a matter of a separate paper (Claret 2000).

Table 1. Limb-Darkening coefficients for $uvbyUBVRIJHK$ bands (Least-Squares Method)

Name	Source	range T_{eff}	range log g	log [M/H]	Vel Turb.	Kind of fitting
Table2	ATLAS	3500 K–50000 K	0.0–5.0	–5.0	2 km/s	Eq. 6, 12 filters
Table3	ATLAS	3500 K–50000 K	0.0–5.0	–4.5	2 km/s	Eq. 6, 12 filters
Table4	ATLAS	3500 K–50000 K	0.0–5.0	–4.0	2 km/s	Eq. 6, 12 filters
Table5	ATLAS	3500 K–50000 K	0.0–5.0	–3.5	2 km/s	Eq. 6, 12 filters
Table6	ATLAS	3500 K–50000 K	0.0–5.0	–3.0	2 km/s	Eq. 6, 12 filters
Table7	ATLAS	3500 K–50000 K	0.0–5.0	–2.5	2 km/s	Eq. 6, 12 filters
Table8	ATLAS	3500 K–50000 K	0.0–5.0	–2.0	2 km/s	Eq. 6, 12 filters
Table9	ATLAS	3500 K–47500 K	0.0–5.0	–1.5	2 km/s	Eq. 6, 12 filters
Table10	ATLAS	3500 K–50000 K	0.0–5.0	–1.0	2 km/s	Eq. 6, 12 filters
Table11	ATLAS	3500 K–50000 K	0.0–5.0	–0.5	2 km/s	Eq. 6, 12 filters
Table12	ATLAS	3500 K–50000 K	0.0–5.0	–0.3	2 km/s	Eq. 6, 12 filters
Table13	ATLAS	3500 K–50000 K	0.0–5.0	–0.2	2 km/s	Eq. 6, 12 filters
Table14	ATLAS	3500 K–50000 K	0.0–5.0	–0.1	2 km/s	Eq. 6, 12 filters
Table15	ATLAS	3500 K–50000 K	0.0–5.0	0.0	2 km/s	Eq. 6, 12 filters
Table16	ATLAS	3500 K–50000 K	0.0–5.0	+0.1	2 km/s	Eq. 6, 12 filters
Table17	ATLAS	3500 K–50000 K	0.0–5.0	+0.2	2 km/s	Eq. 6, 12 filters
Table18	ATLAS	3500 K–50000 K	0.0–5.0	+0.3	2 km/s	Eq. 6, 12 filters
Table19	ATLAS	3500 K–45000 K	0.0–5.0	+0.5	2 km/s	Eq. 6, 12 filters
Table20	ATLAS	3500 K–40000 K	0.0–5.0	+1.0	2 km/s	Eq. 6, 12 filters
Table21	ATLAS	3500 K–50000 K	0.0–5.0	0.0	0 km/s	Eq. 6, 12 filters
Table22	ATLAS	3500 K–50000 K	0.0–5.0	0.0	1 km/s	Eq. 6, 12 filters
Table23	ATLAS	3500 K–50000 K	0.0–5.0	0.0	4 km/s	Eq. 6, 12 filters
Table24	ATLAS	3500 K–50000 K	0.0–5.0	0.0	8 km/s	Eq. 6, 12 filters
Table25 (Sun)	ATLAS	5777 K	4.377	0.0	1.5 km/s	Eq. 6, 12 filters
Table26 (Vega)	ATLAS	9400 K	3.90	–0.5	0 km/s	Eq. 6, 12 filters
Table27 (Sun)	ATLAS	5777 K	4.377	0.0	1.5 km/s	Eq. 6, monochromatic
Table28 (Vega)	ATLAS	9400 K	3.90	–0.5	0 km/s	Eq. 6, monochromatic
Table29	ATLAS	3500 K–50000 K	0.0–5.0	all metallicities	0, 1, 2, 4, 8 km/s	Eq. 6, bolometric
Table30	ATLAS	3500 K–50000 K	0.0–5.0	all metallicities	0, 1, 2, 4, 8 km/s	Eq. 1, 12 filters
Table31	ATLAS	3500 K–50000 K	0.0–5.0	all metallicities	0, 1, 2, 4, 8 km/s	Eq. 2, 12 filters
Table32	ATLAS	3500 K–50000 K	0.0–5.0	all metallicities	0, 1, 2, 4, 8 km/s	Eq. 3, 12 filters
Table33	ATLAS	3500 K–50000 K	0.0–5.0	all metallicities	0, 1, 2, 4, 8 km/s	Eq. 4, 12 filters
Table34	ATLAS	3500 K–50000 K	0.0–5.0	all metallicities	0, 1, 2, 4, 8 km/s	Eq. 1, bolometric
Table35	ATLAS	3500 K–50000 K	0.0–5.0	all metallicities	0, 1, 2, 4, 8 km/s	Eq. 2, bolometric
Table36	ATLAS	3500 K–50000 K	0.0–5.0	all metallicities	0, 1, 2, 4, 8 km/s	Eq. 3, bolometric
Table37	ATLAS	3500 K–50000 K	0.0–5.0	all metallicities	0, 1, 2, 4, 8 km/s	Eq. 4, bolometric
Table38	PHOENIX	2000 K–9800 K	3.5–5.0	0.0	2 km/s	Eq. 6, 12 filters
Table39	PHOENIX	2000 K–9800 K	3.5–5.0	0.0	2 km/s	Eq. 6, bolometric
Table40	PHOENIX	2000 K–9800 K	3.5–5.0	0.0	2 km/s	Eq. 1, 12 filters
Table41	PHOENIX	2000 K–9800 K	3.5–5.0	0.0	2 km/s	Eq. 2, 12 filters
Table42	PHOENIX	2000 K–9800 K	3.5–5.0	0.0	2 km/s	Eq. 3, 12 filters
Table43	PHOENIX	2000 K–9800 K	3.5–5.0	0.0	2 km/s	Eq. 4, 12 filters
Table44	PHOENIX	2000 K–9800 K	3.5–5.0	0.0	2 km/s	Eq. 1, bolometric
Table45	PHOENIX	2000 K–9800 K	3.5–5.0	0.0	2 km/s	Eq. 2, bolometric
Table46	PHOENIX	2000 K–9800 K	3.5–5.0	0.0	2 km/s	Eq. 3, bolometric
Table47	PHOENIX	2000 K–9800 K	3.5–5.0	0.0	2 km/s	Eq. 4, bolometric

Fig. 8. Upper panels: The F'/F test for some selected models as a function of the wavelength and log g. Lower panels: the deviation of the intensity (model-fitted) at $\mu = 0.005$ computed using LSM (dashed) and FCM (continuous, Eq. 4). PHOENIX models.

References

Alcock C., et al., 1997, ApJ 491, 436

Allard F., Hauschildt P.H., 1995, ApJ 445, 433

Allard F., Hauschildt P.H., Alexander D.R., Starrfield S., 1997, ARA&A 35, 137

Allen C.W., 1976, Astrophysical Quantities. 3rd. Edition, Athlone Press, London

Alonso A., Arribas S., Martínez-Roger C., 1994, A&AS 107, 365

Bessel M.S., 1990, PASP 102, 1181

Buerger P., 1972, ApJ 177, 657

Claret A., 1998, A&A 335, 647

Claret A., 2000, in preparation

Claret A., Giménez A., 1990, A&A 230, 412

Claret A., Giménez A., 1992, A&A 256, 572

Claret A., Díaz-Cordovés J., Giménez A., 1995, A&AS 114, 247

Díaz-Cordovés J., 1990, Ph.D. Thesis, Univ. Complutense, Madrid

Díaz-Cordovés J., Giménez A., 1992, A&A 259, 227

Díaz-Cordovés J., Claret A., Giménez A., 1995, A&AS 110, 329

Giménez A., Claret A., 1989, In: Batten A.H. (ed.) Algols. IAU Coll. No. 107, Kluwer, p. 343

Grygar J., 1965, Bull. Astron. Inst. Czech. 16,, 195

Grygar J., Cooper M.L., Jurkevich I., 1972, Bull. Astron. Inst. Czech. 23, 147

Hauschildt P.H., 2000, private communication

Hauschildt P.H., Baron E., Allard F., 1997a, ApJ 483, 390

Hauschildt P. H., Allard F., Alexander D.R., Baron E., 1997b, ApJ 488, 428

Klinglesmith D.A., Sobieski S., 1970, AJ 75, 175

Kurucz R.L., 1979, ApJS 40, 1

Kurucz R.L. 2000, private communication

Manduca, A., Bell R.A., Gustafsson B., 1977, A&A 61, 809

Mazeh T., et al., 2000, ApJ 532, 55

Milne E.A., 1921, MNRAS 81, 361

Peletier R., 1994, private communication

Van Hamme W., 1993, AJ 106, 2096

Wade R.A., Ruciński S.M., 1985, A&AS 60, 471